Husimi-cactus approximation study on the diluted spin ice

Hiromi Otsuka,[1] Yutaka Okabe,[1] and Konstantin Nefedev[2,3]
[1]*Department of Physics, Tokyo Metropolitan University, Tokyo 192-0397, Japan*
[2]*School of Natural Sciences, Far Eastern Federal University, Vladivostok 690091, Russian Federation*
[3]*Institute of Applied Mathematics, Far Eastern Branch, Russian Academy of Science, Vladivostok 690041, Russian Federation*

(Received 14 February 2018; published 27 April 2018)

We investigate dilution effects on the classical spin-ice materials such as $Ho_2Ti_2O_7$ and $Dy_2Ti_2O_7$. In particular, we derive a formula of the thermodynamic quantities as functions of the temperature and a nonmagnetic ion concentration based on a Husimi-cactus approximation. We find that the formula predicts a dilution-induced crossover from the cooperative to the conventional paramagnets in a ground state, and that it also reproduces the "generalized Pauling's entropy" given by Ke *et al.* To verify the formula from a numerical viewpoint, we compare these results with Monte Carlo simulation calculation data, and then find good agreement for all parameter values.

DOI: 10.1103/PhysRevE.97.042132

I. INTRODUCTION

The pyrochlore lattice consisting of corner-sharing tetrahedra is one of the most important structures in condensed matter physics because the geometrical frustrations inhibit the stabilization of a magnetic order in the pyrochlore compounds, which then provide an opportunity for research on unconventional phases and exotic excitations [1,2]. The so-called spin-ice materials $Ho_2Ti_2O_7$ and $Dy_2Ti_2O_7$ are examples of pyrochlores [3–5]; despite their large magnetic moments $\mu \simeq 10\mu_B$, the experiments cannot find any ordered phases, but the ice-type degeneracy in the ground state is found instead [6,7]. Furthermore, with the proposal [8] and the observation [9] of magnetic monopole-like excitations in the spin-ice materials, intensive investigations have been carried out to account for their static and dynamical properties [10–17].

Recently, the diluted spin-ice materials $(R_{1-x}Y_x)_2Ti_2O_7$ (R = Dy or Ho) that the magnetic ions R^{3+} on the pyrochlore lattice Λ_p are substituted for by the nonmagnetic ions Y^{3+} were synthesized in some groups, and on which detailed measurements were performed [18–20]. They reported, for instance, the nonmonotonic dependence of the residual entropy on the nonmagnetic ion density, and discussed its relevance to the generalized formula of Pauling's entropy [18]. Moreover, an intriguing theoretical proposal that a new type of spin glass state emerges by disorder effects on the liquidity of the so-called Coulomb phase was made [21]. Therefore, the diluted materials break new ground in the research of the dilution-induced phenomena observed in the spin-ice systems [22,23].

In this paper, we consider the nearest-neighbor spin-ice model with dilution, whose Hamiltonian, including the Zeeman energy, is as follows:

$$H = -3J \sum_{\langle p,p' \rangle} \tilde{\mathbf{S}}_p \cdot \tilde{\mathbf{S}}_{p'} - \sum_p \tilde{\mathbf{S}}_p \cdot \mathbf{H}, \tag{1}$$

where $\tilde{\mathbf{S}}_p = c_p \mathbf{S}_p$ ($p \in \Lambda_p$) and $\mathbf{S}_p$ is the magnetic moment of the rare-earth ion. To represent the site dilution, we introduced the quenched random variable c_p (=0 or 1) which obeys the probability distribution $\Pr(c_p) = x\delta_{c_p,0} + (1-x)\delta_{c_p,1}$ (where δ is Kronecker's delta) [24]. Thus, $x \in [0,1]$ means the density of the nonmagnetic ions. Due to the crystal field effects, each magnetic moment exhibits a local easy axis anisotropy; namely, if we denote the unit vectors parallel to the edges of the diamond lattice Λ_d (whose medial lattice is Λ_p) as $\mathbf{u}_p$, then $\mathbf{S}_p = \sigma_p \mathbf{u}_p$ ($\sigma_p = \pm 1$). Because $\mathbf{u}_p \cdot \mathbf{u}_{p'} = -\frac{1}{3}$ for nearest-neighboring sites $p, p' \in \Lambda_p$, Eq. (1) gives the diluted antiferromagnetic (AF) Ising model with the coupling $J > 0$. In the following discussion, we treat the magnetic field in the [100] direction. That is, we suppose that $\mathbf{H}$ is parallel to one of the cubic cell axes, e.g., $\mathbf{H} \parallel \mathbf{e}_z$. Then, we define $h = |\mathbf{u}_p \cdot \mathbf{H}| = H/\sqrt{3}$.

For the pure case $x = 0$, the ground state of Eq. (1) consists of the "two-in–two-out" tetrahedra; this shows the ice-type degeneracy [7] and the algebraic decay of spin correlations characterizing the Coulomb phase [25]. At finite temperature T, the defects to represent the breaking of the ice rule behave as emergent particles diffusively moving on Λ_d [8,9]; we define their charges as $q_d = \eta_d \sum_{p \in \{p(d)\}} \sigma_p$ ($d \in \Lambda_d$), where $\{p(d)\}$ and $\eta_d = \pm 1$ represent four corner sites of the dth tetrahedron and the sublattice-dependent sign factor, respectively (i.e., $q_d = \pm 2$ and ± 4 for $x = 0$). For the Coulomb phase, their effects are relevant and yield an off-critical one. Conversely, for the case $x \neq 0$, the tetrahedra including diluted sites may play a role in quenched defects also disturbing spin correlations, and may bring about the paramagnetic phase. In the following, we provide a formula that is based upon the Husimi-cactus approximation (HCA) of corner-sharing tetrahedra [26,27] and predict, for instance, the dilution-induced crossover from the cooperative to the conventional paramagnets even at $T = 0$. To proffer evidence of these predictions, we perform the Monte Carlo (MC) calculations; in doing them, we extend a cluster algorithm of the MC simulation [28] to be adaptable for the diluted spin ice.

Here, we should note that the nearest-neighbor spin-ice model has been employed despite the long-range dipolar interaction being non-negligible for quantitative arguments on experiments [29,30]. As one can see below, this is because the model permits us to accurately treat the dilution effects on

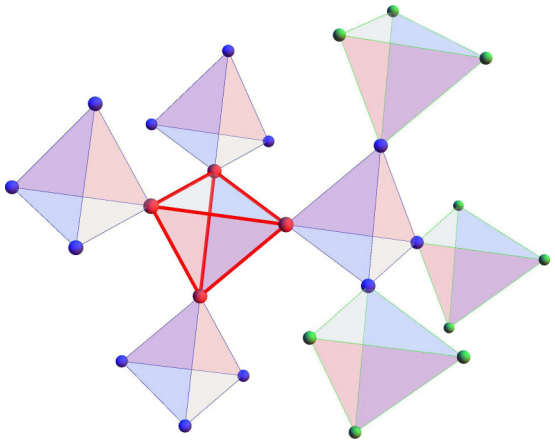

FIG. 1. The Husimi-cactus construction for $\Lambda_{\rm p}$. The four red sites in the central tetrahedron (shown with bold lines) form a red shell, whereas the 12 blue sites in four tetrahedra connected to the red shell form a blue shell. Similarly, the 36 green sites in 12 tetrahedra connected to the blue shell (only a quarter of them are depicted) form a green shell. Then, the Bethe tree $\Lambda_{\rm B}$ draws lines through the centers of the tetrahedra, and represents the shell structure of the tetrahedra constructed, as above.

the spin ice by analytical and numerical methods. Moreover, our treatment can capture the main qualitative features of experiments, which thus can provide a basic understanding of the dilution effects commonly observed in a group of pyrochlore magnets [18–20,31].

II. HUSIMI CACTUS OF TETRAHEDRA

For the pure case, Jaubert *et al.* applied the Husimi-cactus approximation and succeeded in describing properties of the spin ice including the ground-state Kasteleyn transition driven by the magnetic field in the [100] direction [11,14,32]. We thus extend their argument to incorporate the effects of the quenched randomness on the pyrochlore magnets obeying the ice rule.

First, we explain the Husimi cactus of corner-sharing tetrahedra, which is illustrated in Fig. 1. As on $\Lambda_{\rm p}$, each existing tetrahedron is connected to four others. However, there are no closed loops of tetrahedra. Therefore, the Husimi cactus for $\Lambda_{\rm p}$ is isomorphic to the Bethe tree with four neighbors $\Lambda_{\rm B}$, where the center tetrahedron and the four parts jointed to it at the red sites correspond to a center site and four branches of $\Lambda_{\rm B}$, respectively. The Husimi-cactus approximation means to treat Eq. (1) defined on the medial lattice of $\Lambda_{\rm B}$ instead of $\Lambda_{\rm p}$.

Then, our ansatz for the quenched average of the diluted spin ice is expressed as follows [33]:

$$\ln Z(x,T,h) = \sum_{l=0}^{4} B_l(4,x) \ln Z_l, \tag{2}$$

where $B_l(4,x) = \binom{4}{l} x^l (1-x)^{4-l}$ is a probability that the tetrahedron includes l diluted sites; i.e., l obeys the binomial distribution $l \sim B(4,x)$. Z_l represents a partition function of a tree consisting of the center tetrahedron with l diluted sites and $4-l$ jointed branches. This ansatz means that the partition functions Z_l depend not on the diluted-site configurations, but only on their numbers l. We attain this condition by (if necessary) taking an average of the dependence over the diluted-site configurations under a given l. When we denote a partition function of one branch with the spin on the joint site satisfying $\mathbf{S}\cdot\mathbf{H} = h$ as $U(x,T,h)$ [$\mathbf{S}\cdot\mathbf{H} = -h$ as $D(x,T,h)$], owing to the Bethe tree structure, explicit expressions on Z_l are given in their terms, e.g., $Z_1 = u(U^3 + D^3) + (2u + u^{-3})(U^2 D + U D^2)$, where $u := e^{\beta J}$, but the Zeeman energy factor $v := e^{\beta h}$ was merged into U and D. One can find an expression of Z_0 in Ref. [32], and also those of Z_l in the Appendix.

Now, we give the caution on boundary effects in the calculations using the Bethe tree. Because the number of boundary sites is extensive [34], any measurements of physical quantities O on a whole system suffer from strong boundary effects. To circumvent them, we focus on the center tetrahedron: Because the expressions of Z_l retain some statistical mechanical information of $(4-l)$-spin states in the center tetrahedron with l diluted sites, we can read off a contribution O_l to calculate the physical quantities as

$$O(x,T,h) = \sum_{l=0}^{4} B_l(4,x) O_l. \tag{3}$$

Because O_l is expressed as a ratio of $(4-l)$th-order homogeneous polynomials, instead of U and D, their ratio $Y = D/U$ is enough to calculate physical quantities [32]. For example, the uniform magnetization in the $\mathbf{e}_z$ direction can be calculated as $M(x,T,h) = \sum_{l=0}^{4} B_l(4,x) M_l$, where $M_l := (\partial/\partial \ln U - \partial/\partial \ln D) \ln Z_l$ in units of $1/\sqrt{3}$ (explicit expressions are summarized in the Appendix). One can see that this formula satisfies the symmetry property of $M = 0$ at $h = 0$, because the partition functions should be equal, and thus $Y = 1$ for $h = 0$.

To proceed, let us examine U and D. These satisfy recursion relations that are conveniently represented by introducing shell indices of $\Lambda_{\rm B}$, i.e., $U^{(n)}$, $D^{(n)}$, and $Y^{(n)}$. Following Ref. [32], we suppose that n decreases with going to the outer shells of $\Lambda_{\rm B}$ (see Fig. 1) and is zero at the shell of boundary sites. Then, using the same quenched average ansatz with Eq. (2), we can represent the relations as

$$\ln U^{(n+1)} = \sum_{l=0}^{3} B_l(3,x) \ln X_l(U^{(n)}, D^{(n)}) + \ln v, \tag{4}$$

$$\ln D^{(n+1)} = \sum_{l=0}^{3} B_l(3,x) \ln X_l(D^{(n)}, U^{(n)}) - \ln v, \tag{5}$$

where $B_l(3,x) = \binom{3}{l} x^l (1-x)^{3-l}$ is the probability that the tetrahedron with one spin in a fixed direction includes l diluted sites, i.e., $l \sim B(3,x)$. These couple of equations are invariant under the interchange $U \leftrightarrow D$ accompanied by $v \leftrightarrow v^{-1}$ due to the symmetry of the system in Eq. (1). After a small calculation, one obtains $X_l(U,D)$, e.g., $X_1(U,D) = uU^2 + \frac{1}{3}(2u + u^{-3})(2UD + D^2)$. As a result, we find the recursion relations for $Y^{(n)}$ to be

$$\ln Y^{(n+1)} = \sum_{l=0}^{3} B_l(3,x) \ln \psi_l(Y^{(n)}) - 2 \ln v, \tag{6}$$

where $\psi_l(Y) := X_l(D,U)/X_l(U,D)$, and, for instance,

$$\psi_1(Y) = \frac{3uY^2 + (2u+u^{-3})(2Y+1)}{3u + (2u+u^{-3})(2Y+Y^2)}.$$

To obtain a stationary solution of Eq. (6), we numerically evaluate its asymptotic behavior in large n under the initial condition $Y^{(0)}(x,T,h) = 1$, where the magnetic field is zero on the boundary sites. Then, we find that it does converge, i.e., $Y^* = \lim_{n\to\infty} Y^{(n)}$. As expected, for $h = 0$, Eq. (6) results in giving $Y^* = 1$ for all x and T, which implies that the system is in the paramagnetic phase and does not exhibit a magnetic phase transition [35]. In Fig. 2, we give the values of the stationary solution $\ln Y^*(x,T,h)$ in a color map for $x = 0.0$, 0.1, 0.3, and 0.5, as examples. While these data are necessary for investigations of diluted pyrochlores in a magnetic field (we discuss this issue elsewhere), we concentrate on the $h = 0$ case and employ the stationary solution $Y^*(x,T,0) = 1$ in the following (see also Sec. IV).

As an example of physical quantities, we first consider the uniform magnetic susceptibility: $3T\chi = \partial M/\partial \ln v|_{v=1} = \sum_{l=0}^{4} B_l(4,x) 3T\chi_l$, where $3T\chi_l := \partial M_l/\partial Y|_{Y=Y^*} \times \partial Y/\partial \ln v|_{v=1}$. Because the second factor is determined via Eq. (6), one can find the HCA result of $3T\chi$:

$$3T\chi_l = \left.\frac{2\partial M_l/\partial Y}{\sum_{j=0}^{3} B_l(3,x)(\partial\psi_j/\partial Y - 1)}\right|_{Y=Y^*}. \tag{7}$$

In particular, in the pure case, our formula reduces to

$$3T\chi = \left.\frac{2\partial M_0/\partial Y}{\partial\psi_0/\partial Y - 1}\right|_{Y=Y^*} = \frac{8(u^2+1)}{u^2+2+u^{-6}},$$

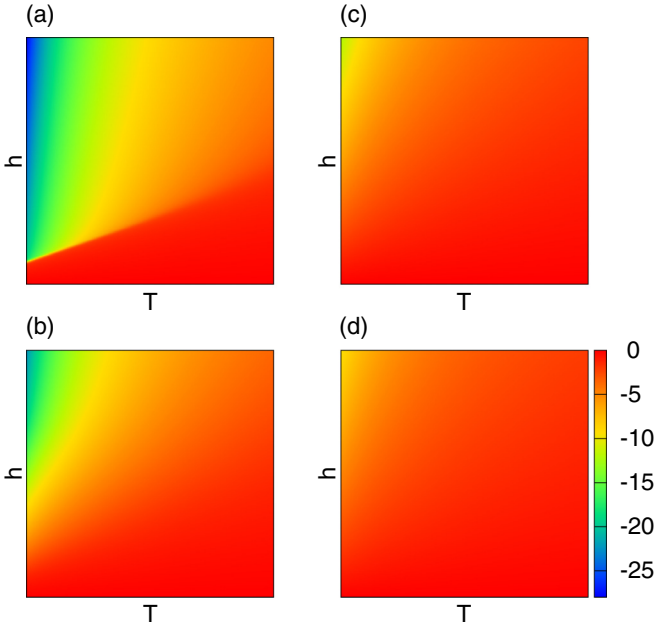

FIG. 2. The color map of the stationary solution $\ln Y^*(x,T,h)$ for $x =$ (a) 0.0, (b) 0.1, (c) 0.3, and (d) 0.5. The horizontal and the vertical directions indicate $T \in [0.1,0.5]$ and $h \in [0.0,0.4]$, respectively. Note that $\ln Y^*(x,T,-h) = -\ln Y^*(x,T,+h)$, so only the case $h > 0$ was plotted.

which is the known result given by Jaubert *et al.* [14]. Also, the low-T limit is of importance to characterize the dilution effects on the cooperative paramagnetic phase of the spin ice [10]. The Curie constant per spin is extracted as $3C_{\rm Curie} = \lim_{T\to 0} 3T\chi/4/(1-x) = 6/(2x^3-2x^2+x+2) - 1$ and exhibits a decrease from 2 to 1 with an increase of x. In the following, we also check this dilution-induced crossover to a conventional paramagnet by using the numerical simulation.

Next, we consider the defect number density $n(x,T)$ whose HCA is given by an average of $|q_d|$ at the center tetrahedron. Suppose that $n(x,T) = \sum_{l=0}^{4} B_l(4,x) n_l$; then, immediately, we obtain

$$n_0 = \frac{4(2+u^{-6})}{3u^2+4+u^{-6}}, \quad n_1 = \frac{3(u+u^{-3})}{3u+u^{-3}},$$
$$n_2 = \frac{2u^{-1}}{u+u^{-1}}, \quad n_3 = 1, \quad \text{and} \quad n_4 = 0. \tag{8}$$

This expression (for instance n_1) possesses expected behaviors in high-T ($n_1 \to \frac{3}{2}$) and low-T ($n_1 \to 1$) limits. One can see that $n(x,0)$ is symmetric about $x = \frac{1}{2}$, which is a consequence of the ice-type constraint.

Similarly, the internal energy and the specific heat are given, respectively, as $E(x,T) = \sum_{l=0}^{4} B_l(4,x) E_l$ with $E_l = -\partial \ln Z_l^*/\partial \ln u$ and $C(x,T) = \sum_{l=0}^{4} B_l(4,x) C_l$ with

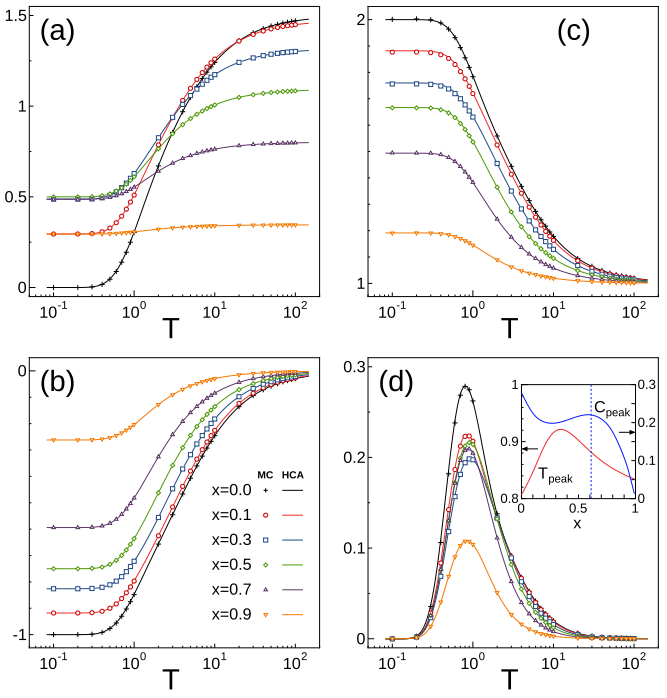

FIG. 3. The comparison of the HCA results (solid curves) and the MC data (marks) of the T dependence of (a) $n(x,T)$, (b) $E(x,T)$, (c) $3T\chi(x,T)$, and (d) $C(x,T)$; the statistical errors are roughly within the mark size. We plot the values of the defect number per tetrahedron, and those of other quantities per spin. The correspondence of values of x with the colors and the marks is given in (b). The inset of (d) gives the HCA results of the peak temperature of the specific heat $T_{\rm peak}$ and the peak height $C_{\rm peak} = C(x,T_{\rm peak})$. The vertical dotted line indicates $x \simeq 0.61$ (see text).

$T^2C_l = -\partial E_l/\partial \ln u$ (we denoted the partition function for the stationary solution as Z_l^*). The straightforward calculation gives E_l and T^2C_l (see the Appendix) as follows:

$$E_0 = \frac{8(1+u^{-6})}{3u^2+4+u^{-6}} - 2, \quad E_1 = \frac{4u^{-3}}{3u+u^{-3}} - 1,$$
$$E_2 = \frac{2u^{-1}}{u+u^{-1}} - 1, \quad \text{and} \quad E_{3,4} = 0. \tag{9}$$

At this stage, we consider the residual entropy per tetrahedron to connect our result with previous calculations [7,18]. When we write the first term of E_l as E_l^{thermal} to denote a thermal energy measured from the ground-state energy (the second term), our formula derives the entropy difference as $S(x,\infty) - S(x,0_+) = \sum_{l=0}^{4} B_l(4,x)\Delta S_l$ with

$$\Delta S_l = \int_0^\infty \frac{C_l}{T}\mathrm{d}T = \int_0^\infty E_l^{\text{thermal}}\mathrm{d}\ln u. \tag{10}$$

Then, one can perform the integrals on the right-hand side, and find that $\Delta S_0 = \ln\frac{8}{3}$, $\Delta S_1 = \ln\frac{4}{3}$, $\Delta S_2 = \ln 2$, and $\Delta S_{3,4} = 0$, respectively. As a result, the residual entropy per spin is given by $S_{\text{res}}(x) = \ln 2 - [1/2/(1-x)]\sum_{l=0}^{4} B_l(4,x)\Delta S_l$, which reproduces the result given by Ke *et al.* [18] and, of course, Pauling's entropy $S_{\text{res}}(0) = \frac{1}{2}\ln\frac{3}{2}$ [7]. In Fig. 3, we provide the curves of the T dependence of $n(x,T)$, $E(x,T)$, $3T\chi(x,T)$, and $C(x,T)$ for several values of x.

III. MONTE CARLO SIMULATIONS

As mentioned in the above, we first extend the loop-string algorithm [28,36] to be adaptable for the diluted spin ice. This extension is done in an *additive* manner to the original algorithm: Imagine that the diluted tetrahedra are randomly distributed on Λ_{d}, and let us denote a set of those with l-diluted sites as $\{d_l\}$. Then, we can apply the original algorithm for $\{d_0\}$, but we do nothing for $\{d_3\}$ and $\{d_4\}$ because they do not have interaction energy. Further, for $\{d_2\}$, two Ising spins in a tetrahedron can be treated by the Swendsen-Wang algorithm [37], where two spins are bonded together with the probability $1-u^{-2}$, if they form a one-in–one-out pair. For the remaining tetrahedra $\{d_1\}$, we should consider a decomposition equation of the Boltzmann weights for three frustrated Ising spins at the corners of a triangular plaquette [38,39]. Additionally, for these remaining tetrahedra, we bond a one-in–one-out pair with a certain probability: To make this concrete, we refer to the left-handpanel of Fig. 1 in Ref. [28] and borrow the definitions of the states and the graphs therein under an assumption that the apex site is diluted. The eight states form two multiplets $(S_0^2,\ldots,S_5^2)$ with $-J$ and (S_0^0,S_0^4) with $+3J$; we thus employ two types of graphs, namely one zero-bond graph G_0^0 and three one-bond graphs G_0^1, G_2^1, and G_4^1; their compatibility condition $\Delta(S_u^\mu, G_v^\nu)$ (=0 or 1) was given in Ref. [17]. From the symmetry consideration, the graph weights should not depend on the subscript [i.e., $W^\mu := W(G_u^\mu)$], and satisfy $W^0 + 2W^1 = u$ and $W^0 = u^{-3}$. Therefore, we can obtain the probability to bond one of two one-in–one-out pairs as

$$\Pr\left(G_u^1 \middle| S_v^2\right) = \frac{W^1}{u} = \frac{1-u^{-4}}{2}. \tag{11}$$

Consequently, the application of three kinds of algorithms to $\{d_0\}$, $\{d_1\}$, and $\{d_2\}$ yields the random cluster representation [40] of the diluted spin ice. In the following MC simulations, we do not encounter the so-called spin-freezing difficulty (also known as the critical slowing down) that exists in single-spin-flip algorithms (see Ref. [41]). This implies that the dilution effects do not introduce a glassy nature into the present nearest-neighbor spin-ice model [42,43], and the loops and strings properly represent spin correlations in the frustrated random spin system.

Now, we summarize our MC simulation results: The systems simulated are rhombohedral and subject to periodic boundary conditions in all directions. We demonstrate the x and T dependence of the above thermodynamic quantities for systems with the linear dimension $L = 64$ ($|\Lambda_{\text{p}}| = 4\times L^3 = 1{,}048{,}576$). We prepare 128 $\sim$ 256 diluted lattices to control the statistical errors stemming from the random sample averages. In Fig. 3, we provide the results of the T dependence for five dilution parameters $x = 0.1, 0.3, 0.5, 0.7$, and 0.9, and also for the pure case $x = 0$ for comparison [14]. The solid curves exhibit the HCA results derived in the above, and the marks plot the MC data, where the errors are roughly within the mark size. Then, it is clear that the agreements of analytical and numerical results are very good for all parameter values ranging over three decades of T and from weak to strong dilutions. Therefore, we can say that our generalized HCA method provides reliable results and offers a different approach in research on diluted spin ice.

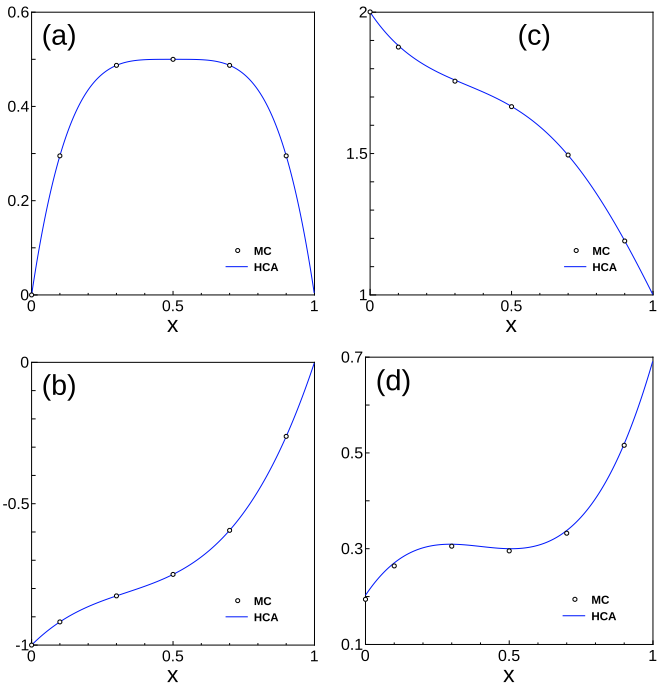

FIG. 4. The comparison of the HCA results (solid curves) and the MC data (open circles) for the ground state, i.e., (a) $n(x,0)$, (b) $E(x,0)$, (c) $3C_{\text{Curie}}(x)$, and (d) $S_{\text{res}}(x)$. We plot the MC data at the lowest temperature simulated ($k_{\text{B}}T = 0.1J$) in (a)–(c), and the estimations by the numerical T integration in (d), respectively. Statistical errors are roughly within the mark size.

Finally, we check our predictions on the ground-state properties. In Fig. 4, we summarize the results of $n(x,0)$, $E(x,0)$, $3C_{\rm Curie}(x)$, and $S_{\rm res}(x)$. With respect to $S_{\rm res}(x)$, two of the present authors carried out the Wang-Landau MC simulations [44] and succeeded in reproducing the generalized Pauling entropy [22]. Nevertheless, for comparison, we also provide MC data in Fig. 4(d), which were obtained by numerical temperature integration of $C(x,T)/T$ given in Fig. 3(d). These exhibit how the HCA method provides an accurate description of the ground-state properties of the diluted spin ice and, in particular, the dilution-induced crossover from the cooperative to the conventional paramagnet that is signaled by the change of the Curie constant from $3C_{\rm Curie} = 2$ to 1 occurring with the increase of the dilution [see Fig. 4(c)]. Simultaneously, we confirm that the spin-freezing difficulty is absent from our ground-state MC simulations using the *generalized* loop-string algorithm proposed in this paper.

IV. DISCUSSION

Based on the HCA, we have investigated the dilution effects on the spin-ice materials. Reflecting the absence of a magnetic phase transition, Eq. (6) yields the ratio of partition functions $Y^* = 1$ as its stationary solution at $H = 0$. Except for the estimation of the magnetic susceptibility, this condition means to treat the pyrochlore as independent tetrahedra: For instance, for the internal energy, Eq. (9) represents the estimates of the single tetrahedron at the center. Nevertheless, our approach provides near-exact results on the thermodynamic quantities evaluated in this research. This may be because the diluted system is deep in the phase with short-range spin correlations, and thus the contributions beyond the single tetrahedron are almost negligible for these quantities. The same situation was already reported for a diluted pyrochlore magnet $SrCr_{9-9x}Ga_{3+9x}O_{19}$, where a cluster calculation also provided reliable results [33].

With respect to the experiments on diluted spin-ice materials $(R_{1-x}Y_x)_2Ti_2O_7$ [18], the dipolar spin-ice (DSI) model with the site dilution has been employed; the MC calculations were performed and succeeded in accurately reproducing the broad peak structure in the specific heat in the wide range of x [19]. For the residual entropy, however, difficulties were experienced in both their MC and the experiments: Due to the spin-freezing dynamics at low T, it is difficult to carry out thermal equilibrium measurements, which thus prevents precise estimation [18,19]. Additionally, DSI was recognized as exhibiting the phase transition to a magnetically ordered state in the pure case [41], and thus the residual entropy, strictly speaking, vanishes at $x = 0$ [45] (also see Ref. [46]). On the one hand, although the present site-diluted nearest-neighbor spin-ice (NSI) model is an oversimplified one, it can qualitatively capture the dilution effects on the spin-ice materials, for instance, for the broad peak structure in the specific heat, the x dependence of the peak temperature $T_{\rm peak}$ and the nonmonotonic behavior of $C_{\rm peak} = C(x,T_{\rm peak})$ [see the inset of Fig. 3(d)] as well as the nonmonotonic behavior of $S_{\rm res}$ in Fig. 4(d). Our formula based on HCA provides analytical expressions of these quantities, which were revealed to be almost exact for NSI via comparisons with MC data; this demonstrates, for instance, that $C_{\rm peak}$ takes a maximum at around the threshold of the site percolation on $\Lambda_{\rm p}$, $p_c = 1 - x \simeq 0.39$ [43,47], which may imply a relevance of the lattice connectivity to this peak formation mechanism. We will report more detailed applications of our approach elsewhere.

To summarize, we studied the diluted spin-ice model by the use of both the Husimi-cactus approximation method and the Monte Carlo method based on the generalized loop-string algorithm. The comparison between them revealed the remarkable accuracy and the qualitative predictability of our formula for physical quantities. Based on our comparison, we clarified the dilution-induced crossover from the cooperative to the conventional paramagnets that may be commonly observed in the spin-ice materials.

ACKNOWLEDGMENTS

We would like to give thanks for stimulating discussions with P. Andriushchenko, K. Soldatov, and A. Peretyatko. Main computations were performed by using facilities at Tohoku University and Tokyo Metropolitan University. This work was supported by JSPS KAKENHI Grant Nos. 26400399 and JP16K05480.

APPENDIX: QUANTITIES USED IN HCA CALCULATIONS

In this Appendix, we write out quantities used (but, not explicitly given) in the Sec. II. It is noted that quantities defined in the text, but not listed below, take zero.

In Eq. (2), we introduced Z_l, which are given as follows:

$$Z_0 = u^2(U^4+D^4) + 4(U^3D + UD^3) + 2(2u^2 + u^{-6})U^2D^2,$$
$$Z_1 = u(U^3 + D^3) + (2u + u^{-3})(U^2D + UD^2),$$
$$Z_2 = \tfrac{1}{3}(2u + u^{-1})(U^2 + D^2) + \tfrac{2}{3}(u + 2u^{-1})UD,$$
$$Z_3 = U + D,$$
$$Z_4 = 1.$$

Below Eq. (3), we defined $M_l(Y)$ as contributions to the uniform magnetic moment, which are given as follows:

$$M_0 = \frac{4u^2(1 - Y^4) + 8(Y - Y^3)}{u^2(1 + Y^4) + 4(Y + Y^3) + 2(2u^2 + u^{-6})Y^2},$$
$$M_1 = \frac{3u(1 - Y^3) + (2u + u^{-3})(Y - Y^2)}{u(1 + Y^3) + (2u + u^{-3})(Y + Y^2)},$$
$$M_2 = \frac{2(2u + u^{-1})(1 - Y^2)}{(2u + u^{-1})(1 + Y^2) + 2(u + 2u^{-1})Y},$$
$$M_3 = \frac{1 - Y}{1 + Y}.$$

The quantities $X_l(U,D)$ and $\psi_l(Y)$ in the recursion relations Eqs. (4)–(6) are given, respectively, as

$$X_0 = u^2U^3 + 3U^2D + (2u^2 + u^{-6})UD^2 + D^3,$$
$$X_1 = uU^2 + \tfrac{1}{3}(2u + u^{-3})(2UD + D^2),$$
$$X_2 = \tfrac{1}{3}(2u + u^{-1})U + \tfrac{1}{3}(u + 2u^{-1})D,$$
$$X_3 = 1,$$

and

$$\psi_0 = \frac{u^2Y^3 + 3Y^2 + (2u^2 + u^{-6})Y + 1}{u^2 + 3Y + (2u^2 + u^{-6})Y^2 + Y^3},$$
$$\psi_1 = \frac{3uY^2 + (2u + u^{-3})(2Y + 1)}{3u + (2u + u^{-3})(2Y + Y^2)},$$
$$\psi_2 = \frac{(2u + u^{-1})Y + (u + 2u^{-1})}{(2u + u^{-1}) + (u + 2u^{-1})Y},$$
$$\psi_3 = 1.$$

The derivatives in Eq. (7) are given as follows:

$$\left.\frac{\partial M_0}{\partial Y}\right|_{Y=1} = -\frac{8(u^2+1)}{3u^2 + 4 + u^{-6}},$$
$$\left.\frac{\partial M_1}{\partial Y}\right|_{Y=1} = -\frac{11u + u^{-3}}{2(3u + u^{-3})},$$
$$\left.\frac{\partial M_2}{\partial Y}\right|_{Y=1} = -\frac{2(2u + u^{-1})}{3(u + u^{-1})},$$
$$\left.\frac{\partial M_3}{\partial Y}\right|_{Y=1} = -\frac{1}{2},$$

and

$$\left.\frac{\partial \psi_0}{\partial Y}\right|_{Y=1} = \frac{u^2 - u^{-6}}{3u^2 + 4 + u^{-6}},$$
$$\left.\frac{\partial \psi_1}{\partial Y}\right|_{Y=1} = \frac{2(u - u^{-3})}{3(3u + u^{-3})},$$
$$\left.\frac{\partial \psi_2}{\partial Y}\right|_{Y=1} = \frac{u - u^{-1}}{3(u + u^{-1})}.$$

In the last paragraph of Sec. II, we defined C_l as contributions to the specific heat, which are given as follows:

$$T^2C_0 = \frac{48(u^2 + 4u^{-4} + 3u^{-6})}{(3u^2 + 4 + u^{-6})^2},$$
$$T^2C_1 = \frac{48u^{-2}}{(3u + u^{-3})^2},$$
$$T^2C_2 = \frac{4}{(u + u^{-1})^2}.$$

[1] P. Anderson, Phys. Rev. **102**, 1008 (1956).
[2] J. S. Gardner, M. J. P. Gingras, and J. E. Greedan, Rev. Mod. Phys. **82**, 53 (2010).
[3] M. J. Harris, S. T. Bramwell, D. F. McMorrow, T. Zeiske, and K. W. Godfrey, Phys. Rev. Lett. **79**, 2554 (1997).
[4] A. P. Ramirez, A. Hayashi, R. Cava, R. Siddharthan, and B. Shastry, Nature (London) **399**, 333 (1999).
[5] S. T. Bramwell, M. J. Harris, B. C. den Hertog, M. J. P. Gingras, J. S. Gardner, D. F. McMorrow, A. R. Wildes, A. Cornelius, J. D. M. Champion, R. G. Melko, and T. Fennell, Phys. Rev. Lett. **87**, 047205 (2001).
[6] J. Bernal and R. Fowler, J. Chem. Phys. **1**, 515 (1933).
[7] L. Pauling, J. Am. Chem. Soc. **57**, 2680 (1935).
[8] C. Castelnovo, R. Moessner, and S. L. Sondhi, Nature (London) **451**, 42 (2008).
[9] H. Kadowaki *et al.*, J. Phys. Soc. Jpn. **78**, 103706 (2009).
[10] I. A. Ryzhkin, J. Exp. Theor. Phys. **101**, 481 (2005).
[11] L. D. C. Jaubert, J. T. Chalker, P. C. W. Holdsworth, and R. Moessner, Phys. Rev. Lett. **100**, 067207 (2008).
[12] T. Fennell *et al.*, Science **326**, 415 (2009).
[13] L. D. C. Jaubert and P. C. W. Holdsworth, J. Phys.: Condens. Matter **23**, 164222 (2011).
[14] L. D. C. Jaubert, M. J. Harris, T. Fennell, R. G. Melko, S. T. Bramwell, and P. C. W. Holdsworth, Phys. Rev. X **3**, 011014 (2013).
[15] H. Takatsu *et al.*, J. Phys. Soc. Jpn. **82**, 073707 (2013).
[16] H. Takatsu *et al.*, J. Phys. Soc. Jpn. **82**, 104710 (2013).
[17] H. Otsuka, H. Takatsu, K. Goto, and H. Kadowaki, Phys. Rev. B **90**, 144428 (2014).
[18] X. Ke, R. S. Freitas, B. G. Ueland, G. C. Lau, M. L. Dahlberg, R. J. Cava, R. Moessner, and P. Schiffer, Phys. Rev. Lett. **99**, 137203 (2007).
[19] T. Lin, X. Ke, M. Thesberg, P. Schiffer, R. G. Melko, and M. J. P. Gingras, Phys. Rev. B **90**, 214433 (2014).
[20] S. Scharffe, O. Breunig, V. Cho, P. Laschitzky, M. Valldor, J. F. Welter, and T. Lorenz, Phys. Rev. B **92**, 180405(R) (2015).
[21] A. Sen and R. Moessner, Phys. Rev. Lett. **114**, 247207 (2015).
[22] Y. Shevchenko, K. Nefedev, and Y. Okabe, Phys. Rev. E **95**, 052132 (2017).
[23] A. Peretyatko, K. Nefedev, and Y. Okabe, Phys. Rev. B **95**, 144410 (2017).
[24] J.-Y. Fortin, J. Phys.: Condens. Matter **25**, 296004 (2013).
[25] C. L. Henley, Annu. Rev. Condens. Matter Phys. **1**, 179 (2010).
[26] K. Husimi, J. Chem. Phys. **18**, 682 (1950).
[27] R. J. Riddell, Jr. and G. E. Uhlenbeck, J. Chem. Phys. **21**, 2056 (1953).
[28] H. Otsuka, Phys. Rev. B **90**, 220406(R) (2014).
[29] B. C. den Hertog and M. J. P. Gingras, Phys. Rev. Lett. **84**, 3430 (2000).
[30] A. Sen, R. Moessner, and S. L. Sondhi, Phys. Rev. Lett. **110**, 107202 (2013).
[31] A. Keren, J. S. Gardner, G. Ehlers, A. Fukaya, E. Segal, and Y. J. Uemura, Phys. Rev. Lett. **92**, 107204 (2004).
[32] L. Jaubert, PhD. thesis, ENS Lyon, 2009 (unpublished).
[33] R. Moessner and A. J. Berlinsky, Phys. Rev. Lett. **83**, 3293 (1999).
[34] R. J. Baxter, *Exactly Solved Models in Statistical Mechanics* (Academic Press, London, 1982).
[35] O. J. Heilmann and E. H. Lieb, Commun. Math. Phys. **25**, 190 (1972).
[36] H. Otsuka, Phys. Rev. B **92**, 134401 (2015).
[37] R. H. Swendsen and J.-S. Wang, Phys. Rev. Lett. **58**, 86 (1987).
[38] D. Kandel and E. Domany, Phys. Rev. B **43**, 8539 (1991).
[39] P. D. Coddington and L. Han, Phys. Rev. B **50**, 3058 (1994).
[40] C. Fortuin and P. Kasteleyn, Physica **57**, 536 (1972).

[41] R. G. Melko, B. C. den Hertog, and M. J. P. Gingras, Phys. Rev. Lett. **87**, 067203 (2001).
[42] J. Villain, Z. Phys. B **33**, 31 (1979).
[43] C. L. Henley, Can. J. Phys. **79**, 1307 (2001).
[44] F. Wang and D. P. Landau, Phys. Rev. Lett. **86**, 2050 (2001).
[45] D. Pomaranski *et al.*, Nat. Phys. **9**, 353 (2013).
[46] P. A. McClarty, O. Sikora, R. Moessner, K. Penc, F. Pollmann, and N. Shannon, Phys. Rev. B **92**, 094418 (2015).
[47] A. Aharony and D. Stauffer, *Introduction to Percolation Theory* (Taylor & Francis, Philadelphia. PA, 2003).